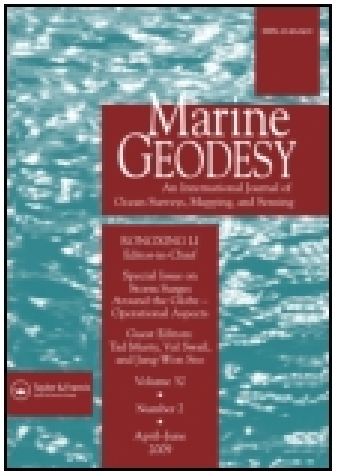

Marine Geodesy
Publication details, including instructions for authors and subscription information:
http://www.tandfonline.com/loi/umgd20

Modeling Uncertainty in Photogrammetry-Derived National Shoreline

Fang Yao[ab], Christopher E. Parrish[ac], Shachak Pe'eri[a], Brian R. Calder[a] & Yuri Rzhanov[a]

[a] Center for Coastal and Ocean Mapping, University of New Hampshire, Durham, New Hampshire, USA

[b] Esri, Redlands, California, USA

[c] School of Civil and Construction Engineering, Oregon State University, Corvallis, Oregon, USA

Published online: 15 Dec 2014.

To cite this article: Fang Yao, Christopher E. Parrish, Shachak Pe'eri, Brian R. Calder & Yuri Rzhanov (2015) Modeling Uncertainty in Photogrammetry-Derived National Shoreline, Marine Geodesy, 38:2, 128-145, DOI: 10.1080/01490419.2014.957792

To link to this article: http://dx.doi.org/10.1080/01490419.2014.957792

Marine Geodesy, 38:128–145, 2015

ISSN: 0149-0419 print / 1521-060X online
DOI: 10.1080/01490419.2014.957792

Taylor & Francis
Taylor & Francis Group

Modeling Uncertainty in Photogrammetry-Derived National Shoreline

FANG YAO,[1,2] CHRISTOPHER E. PARRISH,[1,3] SHACHAK PE'ERI,[1] BRIAN R. CALDER,[1] AND YURI RZHANOV[1]

[1]Center for Coastal and Ocean Mapping, University of New Hampshire, Durham, New Hampshire, USA
[2]Esri, Redlands, California, USA
[3]School of Civil and Construction Engineering, Oregon State University, Corvallis, Oregon, USA

Tidally-referenced shoreline data serve a multitude of purposes, ranging from nautical charting, to coastal change analysis, wetland migration studies, coastal planning, resource management and emergency management. To assess the suitability of the shoreline for a particular application, end users require reliable estimates of the uncertainty in the shoreline position. Previous studies on modeling uncertainty in shoreline mapping from remote sensing data have focused on airborne light detection and ranging; to date, these methods have not been extended to aerial imagery and photogrammetric shoreline mapping, which remains the primary shoreline mapping method used by the National Geodetic Survey. The aim of this article is to develop and test a rigorous total propagated uncertainty model for shoreline compiled from both tide-coordinated and non-tide-coordinated aerial imagery using photogrammetric methods. The uncertainty model is developed using data from a study site in northeast Maine. For the study area, the standard uncertainty was found to be ∼3.2–3.3 m, depending on whether the imagery was tide coordinated or not. The uncertainty model developed in this paper can easily be extended from the study area to other areas and may facilitate estimation of uncertainty in inundation models and marsh migration models.

Keywords National shoreline, photogrammetric stereo compilation, uncertainty

Introduction

Accurately mapped shoreline is important to nautical charting agencies/offices, as well as coastal scientists and coastal zone managers. It supports legal property boundary definition (e.g., Morton and Speed 1998), safe marine navigation, and a wealth of coastal science and resource management applications (e.g., shoreline change, sea-level rise, inundation modeling, habitat change, wetlands studies, restoration, etc.) (e.g., Smith and Zarillo 1990; Leatherman and Anders 1999; Boak and Turner 2005). Currently, one of the missions of the National Geodetic Survey (NGS) of the National Oceanic and Atmospheric

Received 13 June 2014; accepted 19 August 2014.
Address correspondence to Fang Yao, Esri, 380 New York Street, Redlands, CA 92373. E-mail: fangyao.whu@gmail.com
Color versions of one or more of the figures in the article can be found online at www.tandfonline.com/umgd.

Administration (NOAA) is to survey coastal regions in the United States and to provide accurate, consistent, and up-to-date national shoreline (National Geodetic Survey 2014a). Shoreline mapping techniques are developing at a rapid pace. Current remote sensing technologies that can be applied for shoreline mapping include synthetic aperture radar (SAR) (Alfugara et al. 2011), interferometric SAR (InSAR), light detection and ranging (LiDAR) (White et al. 2011), high-resolution commercial satellite imagery (National Geodetic Survey 2014b), and airborne hyperspectral imaging (Graham et al. 2003). However, photogrammetric stereo compilation from aerial imagery remains the primary method used by NGS for mapping the national shoreline.

Although photogrammetric stereo compilation technology is mature, measurement and compilation uncertainties are still not adequately modeled in many applications, including shoreline mapping. This article provides a discussion of uncertainties involved in the photogrammetric shoreline mapping and develops a total propagated uncertainty (TPU) model that can be used to (1) generate accuracy metadata for the national shoreline, (2) determine whether the accuracy of the shoreline satisfies the requirements of International Hydrographic Organization (IHO) S-44 Standards for Hydrographic Surveys (International Hydrographic Organization 2008), (3) help to make informed policy decisions, and (4) enable computation of uncertainty in shoreline change rate estimates and other derived data product.

NGS Shoreline Definition

Shoreline is often defined, for nonscientific purposes, as the line where a body of water and the shore meet. However, due to the dynamic nature of shoreline, this definition is not useful in practice (e.g., in mapping applications and coastal change analysis). There are numerous shoreline indicators that have been used in the shoreline mapping and described in many publications (e.g., Carter et al. 1981; Stafford and Langfelder 1971; Pajak and Leatherman 2002; Boak and Turner 2005), but it is difficult for the practitioners to agree on a common shoreline indicator. All indicators can be divided into two categories: (1) physical shoreline indicators (Stockdon et al. 2002; Boak and Turner 2005), including berm crest, scarp edge, vegetation line, dune toe, dune crest, and cliff or bluff crest and toe; and (2) water-level based shoreline indicators (Shalowitz 1964; Pajak and Leatherman 2002), including high water line, mean high water (MHW) line, mean lower low water (MLLW) line, wet/dry boundary, and wet sand line.

Currently, NGS compiles the MHW line and MLLW line as shoreline indicators to map the national shoreline in order to minimize the tidal daily, monthly and yearly variations (Office of Coast Survey 2014a). MHW and MLLW lines are consistently-defined shorelines, which are designated to be shown on U.S. nautical charts. MHW lines are the legal lines of the United States and the boundaries between land and sea. MLLW lines help to define America's territorial limits, the Exclusive Economic Zone, and the High Seas (Woolard et al. 2003).

NGS Photogrammetric Shoreline Mapping

Stereo photogrammetry controlled by kinematic Global Positioning System (GPS) is a mature and reliable method for mapping the national shoreline. This method can maintain good accuracy for man-made or built-up shoreline, as well as natural shoreline, ranging from mudflats to steep, rocky shoreline. Aerial photogrammetric surveys to map the shoreline are usually performed when the vertical difference between the predicted water level and

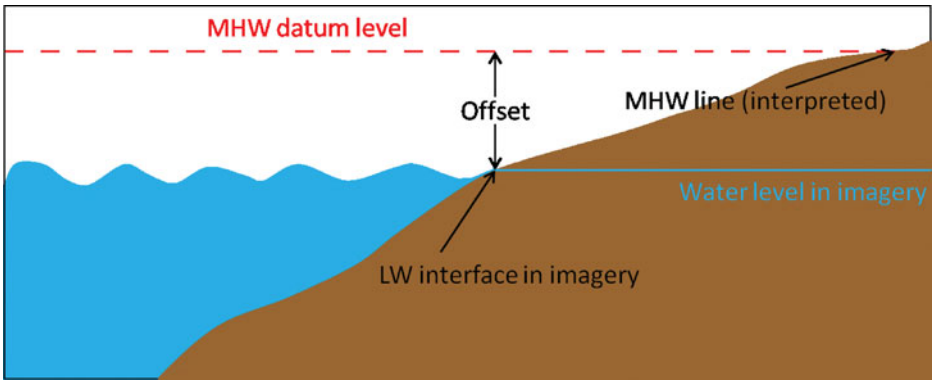

Figure 1. Cross section drawing which shows the relationship between MHW datum and observed water level.

MHW or MLLW is within a specified tolerance, defined by NGS as (Graham et al. 2003):

$$T_r = \begin{cases} \pm 0.09, & r \leq 1.5m \\ \pm 0.1r, & r > 1.5m \end{cases} \quad (1)$$

where T_r is the tolerance in meters and r is the tide range. The land-water interface in tide-coordinated imagery is compiled as the MHW or MLLW line. Near infrared emulsion in film photography, or the NIR band in a digital aerial camera, is typically used for compiling shoreline from tide-coordinated imagery (Li et al. 2002). The reason for this is that radiation at NIR wavelengths is strongly absorbed by water, leading to strong contrast between land and water in the imagery (Smith 1978; Sabins 1986; Parrish et al. 2005).

When it is not possible to collect imagery within the water level tolerance defined by Eq. (1), compliers will delineate the MHW line stereoscopically, based on elevation and water level data. The compilers will first place the photogrammetric floating mark on the ground just landward of land-water interface, then raise the floating mark up by the vertical offset between the MHW datum and observed water level at the time of imagery acquisition and delineate an elevation contour corresponding to the intersection of the MHW datum and terrain surface (Figure 1). This procedure is repeated every few tens of meters along the shoreline (personal communication, Mike Espey, NOAA/NGS/Remote Sensing Division, 2013). Natural color imagery is often used as non-tide-coordinated imagery given that it can provide more indicators to assist in shoreline compilation. The MLLW line is seldom compiled from non-tide-coordinated imagery. In theory it would be possible, but there are fewer opportunities to acquire the imagery when water level is below the MLLW datum (White et al. 2011).

Uncertainty Analysis

Based on NOAA's shoreline mapping procedures, the TPU model is designed to cover two cases: one in which the imagery is tide-coordinated and the other in which it is not.

Shoreline Uncertainty Based on Tide-Coordinated Imagery

When shoreline is compiled from tide-coordinated imagery, the main uncertainty sources include exterior orientation element uncertainty, offset between MHW or MLLW datum and observed water level, water level uncertainty, and human compilation uncertainty.

Exterior orientation element uncertainty. With the availability of integrated global positioning system (GPS)/inertial measurement unit (IMU) systems, direct georeferencing without ground control points has been used increasingly in aerial photogrammetry. NGS currently uses direct georeferencing for certain coastal mapping projects. The component uncertainties when using directly-georeferenced aerial imagery include interior orientation element uncertainty, exterior orientation element uncertainty, and uncertainty of corresponding image point coordinate measurement (Yuan and Zhang 2008). The influence of interior orientation element uncertainty on direct georeferencing accuracy is much smaller than that of exterior orientation element uncertainty, particularly with a well-calibrated camera (Zhang and Yuan 2008). This article focuses on measurement and processing uncertainty, which is treated as first-order uncertainty. Calibration uncertainty is treated as second-order uncertainty and ignored in this article. In addition, the uncertainty of image point coordinate measurement can be treated as part of the human compilation uncertainty, which will be discussed later. Therefore, this section focuses on exterior orientation element uncertainty.

Corresponding rays to the same ground point from two images of a stereo pair must intersect at this point. According to the photogrammetric space intersection theory, the ground point coordinates are determined from camera exterior orientation elements determined from direct georeferencing and corresponding image point coordinates. With three unknowns (the ground point coordinates X, Y, and Z) and four equations, the least square method is applied. Conventional (i.e., analytical) methods of uncertainty propagation can become extremely unwieldy in the case that the final coordinates are obtained from least square adjustments of (redundant) sets of linearized photogrammetric collinearity condition equations. In cases where analytical uncertainty propagation is disadvantageous, Monte Carlo methods are a preferred alternative (Papadopoulos and Yeung 2001). The concept behind the Monte Carlo method is to generate a large number of experimental trials from which the distribution function of the output quantity can be estimated. Given that the ground point coordinate uncertainties for different stereo image pairs from the same survey were not much different from one another, the Root Mean Square (RMS) of the uncertainties of each image pair was treated as the final ground point coordinate uncertainties of the survey, rather than considering the uncertainties of each image pair separately. The Monte Carlo method used in this study is illustrated graphically in Figure 2.

Although the computation result was more accurate with the increase of Monte Carlo simulation trials, increasing the number of trials also increased the computation time. In order to ensure efficiency and accuracy at the same time, the simulation times of each pair of corresponding image points were adjusted based on the number of the image pairs: 2,000 divided by the number of the image pairs. It was found that the computation time was about five seconds on a Windows PC with a 2.5 GHz processor and 6 GB of RAM, and the accuracy was greater than 0.005 m for X and Y uncertainties and 0.02 m for Z uncertainty.

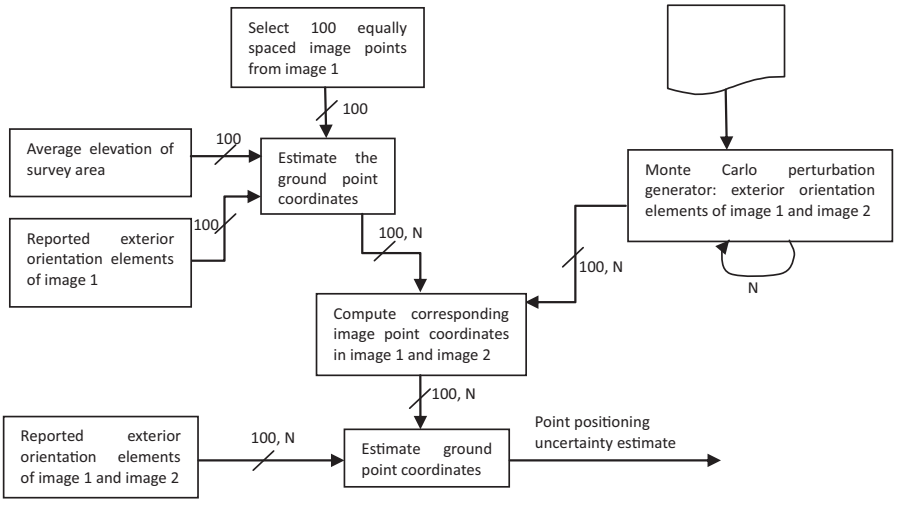

Figure 2. Configuration of the Monte Carlo analysis method for determining positioning uncertainty caused by exterior orientation element uncertainty for each image pair.

Distance root mean square (DRMS) was then computed as the position uncertainty caused by exterior orientation element uncertainty according to the formula

$$DRMS = \sqrt{\sigma_x^2 + \sigma_y^2} \tag{2}$$

where σ_x and σ_y are the standard uncertainty of X and Y coordinates, respectively.

Offset between MHW or MLLW datum and observed water level. Although tide-coordinated imagery is acquired when the offset between MHW or MLLW datum and observed water level is within the specified tolerance, it is unlikely that the observed water level will coincide exactly with the MHW or MLLW datum surface. Therefore, the resulting vertical offset introduces uncertainty in the final shoreline product.

NOAA's Center for Operational Oceanographic Products and Services (CO-OPS) uses Tide Constituent and Residual Interpolation (TCARI) (Hess et al. 1999) and discrete tidal zoning methodologies to enable NGS to acquire tide coordinated imagery. Based on data at tide stations, TCARI uses the Laplace Equation interpolation method to generate spatial weighting functions to interpolate 1) tidal constants for reconstructing astronomic tide, 2) the residual caused by nontidal effects, and 3) the datum offsets between Mean Sea Level (MSL) and MLLW (Cisternelli and Gill 2005; Office of Coast Survey 2014b). These three components are then combined to acquire the water level data at the interested location. If TCARI grids are available, NGS will apply the software Pydro (Office of Coast Survey 2014c) to obtain the instantaneous water level relative to MHW and MLLW at the time of acquisition of each image. Otherwise, CO-OPS will develop discrete tidal zoning schemes. Discrete tidal zoning divides the coastal area of interest into many areas with similar tidal characteristics using polygons, and then apply time and range correctors to the observed water level data from nearby tide stations to acquire the water level at any divided area (CO-OPS 2014).

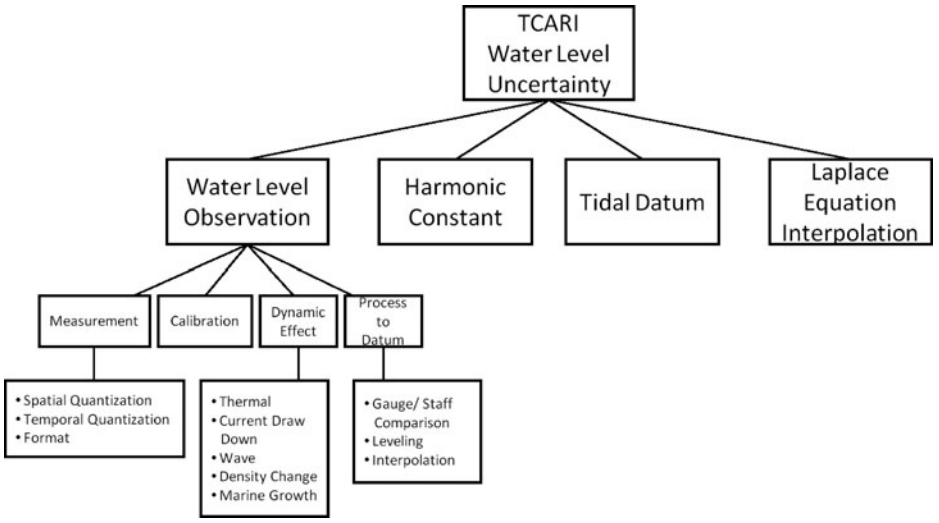

Figure 3. TCARI water level uncertainty (adapted from Brennan 2005).

Water level uncertainty. In the case that a survey area is covered by TCARI grids, the water level uncertainty sources include measurement uncertainty of gauge/sensor and processing uncertainty to refer the measurements to station datum, harmonic constant uncertainty, uncertainty in computation of tidal datum for the adjustment to a 19-year national tidal datum epoch (NTDE) from short-term stations, and Laplace Equation interpolation uncertainty. Figure 3 shows all the contributing elements for TCARI water level uncertainty.

In the case of a survey area covered by discrete tidal zoning schemes, then the uncertainty sources will not include harmonic constant uncertainty and Laplace Equation interpolation uncertainty. Instead, an uncertainty in the application of tidal or water level zoning will be added to uncertainty sources (Gibson and Gill 1999).

Human compilation uncertainty. Compilers interpret the land-water interface as the MHW or MLLW shoreline when the water level is within the specified tolerance at the time of image acquisition, and this minimizes human compilation uncertainty. However, the accuracy of human compilation still depends on many factors, including image quality and the compiler's knowledge, training, and experience. These factors cannot be quantified simply, and thus it is difficult to build an appropriate model to describe human compilation uncertainty. In this study, the shoreline compilation results were analyzed from different compilers to obtain an approximate human compilation uncertainty value.

Total propagated uncertainty. All vertical uncertainty components (the offset between MHW or MLLW datum and observed water level and water level uncertainty) should be converted to the horizontal uncertainty components using the beach slope before calculating the total uncertainty. Then, the total standard uncertainty (at 68% confidence level) and the uncertainty at 95% confidence level are computed using the formulas (each uncertainty component is assumed to be independent with the others):

$$u = S + t_{68,v} R \tag{3}$$

$$U_{95} = S + t_{95,v} R \tag{4}$$

where u is the standard uncertainty (at 68% confidence level); U_{95} is the uncertainty at 95% confidence level; $t_{68,v}$ is the Student's t (or coverage factor) for 68% confidence level and v degrees of freedom; $t_{95,v}$ is the Student's t (or coverage factor) for 95% confidence level and v degrees of freedom, when degrees of freedom are infinite, $t_{68,v}$ and $t_{95,v}$ are 1 and 1.96, respectively; when there are fewer than 30 degrees of freedom, the sample standard deviation is smaller than the population standard deviation, so Student's t is used to compensate for the sample standard deviation (Dieck 2002); S is the sum of all systematic uncertainties, and R is the root sum square of all random uncertainties. The degrees of freedom can be obtained (Dieck 2002):

$$v = \frac{\left[\sum_{i=1}^{N}(r_i)^2 + \sum_{j=1}^{M}\left(s_j/2\right)^2\right]^2}{\left[\sum_{i=1}^{N}\frac{(r_i)^4}{v_i} + \sum_{j=1}^{M}\frac{\left(s_j/2\right)^4}{v_j}\right]} \tag{5}$$

where r_i is the *ith* random uncertainty ($1 \le i \le N$, N is the number of random uncertainty components),v_i is the degrees of freedom for the *ith* random uncertainty, s_j is the *jth* systematic uncertainty component ($1 \le j \le M$, M is the number of systematic uncertainty components), v_j is the degrees of freedom for the *jth* systematic uncertainty.

For tide-coordinated shoreline compilation, the offset between the MHW or MLLW datum and observed water level and the tidal datum uncertainty are treated as systematic uncertainties, while the other uncertainty sources are modeled as random uncertainties.

Shoreline Uncertainty Based on Non-Tide-Coordinated Imagery

When shoreline is compiled from non-tide-coordinated imagery, only three main uncertainty sources contribute to the total uncertainty: (1) exterior orientation element uncertainty, (2) water level uncertainty, and (3) human compilation uncertainty. The analysis methods for the first two are the same as those from tide-coordinated imagery. However, because the compilation from non-tide-coordinated imagery is primarily done based on elevation information, the human compilation uncertainty was analyzed in elevation and then converted back to the uncertainty in the plane by the slope.

For non-tide-coordinated shoreline compilation, only the tidal datum uncertainty is treated as systematic uncertainty, while the other uncertainty sources are modeled as random uncertainties. Equations (3) and (4) are used to compute the total standard uncertainty and the uncertainty at 95% confidence level.

Experimental Results

On 21 June 2011, a NOAA NGS aerial survey (ME1001) was conducted to provide aerial images of the strait that links Dennys Bay, Whiting Bay, and Cobscook Bay in the northeast coastal region of Maine (Figure 4). The region is characterized by a large tide range, strong tidal currents, numerous embayments, and coarse-sediment pocket beaches. The slope of beaches, which was extracted from LiDAR-derived DEM (Coastal Services Center 2014) in ArcGIS, ranges from approximately 1° to 46°, with the average slope being ~14°. In addition to this wide range of slopes, the study site encompasses a number of different types of shoreline, ranging from rock outcrop to gravel pocket beaches and tidal mudflats. The complexity of the site and the range of shoreline types covered were determined to be advantageous for developing the shoreline TPU model. In particular, it should be possible to extend the TPU model and procedures to other survey sites that are less complex and

Table 1
Tide analysis report (provided by NGS)

The center time (GMT) of the flight line	Relative to MLLW (m)				Relative to MHW (m)			
	13:18 50-002	13:24 50-001	14:06 50-001	14:18 50-002	13:18 50-002	13:24 50-001	14:06 50-001	14:18 50-002
Eastport	0.39	0.35	0.33	0.40	−5.34	−5.38	−5.40	−5.33
Coffins Point	0.59	0.58	0.27	0.27	−4.84	−4.84	−5.16	−5.16
Birch Islands	1.10	0.88	0.36	0.30	−4.33	−4.54	−5.07	−5.13

exhibit greater homogeneity of shoreline type, whereas the reverse would not necessarily be true. It is also important to note that, due to the complexity of the shoreline in this region, the shoreline uncertainty is expected to generally be higher than that in other areas.

Seventy natural color and NIR images were taken using an Applanix Digital Sensor System (DSS) 439 DualCam at an altitude of 3048 m along two flight lines 50-001 and 50-002 (each flown twice). The mosaic imagery, the flight lines, and the tide gauges are depicted in Figure 5.

Because TCARI grids were not available for the study site, an NGS compiler performed tidal level calculations by hand and produced a "Tide Analysis Report" (Table 1). The tide gauges used for this survey were Coffins Point and Birch Islands (both subordinate stations), and Eastport (19-year control station) (Figure 5).

Given that the tide tolerance for the two subordinate stations is 0.53 m, two of the four flight lines were out of the MLLW tide tolerance, and all the flight lines were out of the MHW tide tolerance. Thus, the MLLW shorelines were mainly compiled from tide-coordinated imagery, and all the MHW shorelines were from non-tide-coordinated imagery. This situation provided a good test case for this study, since uncertainties in both

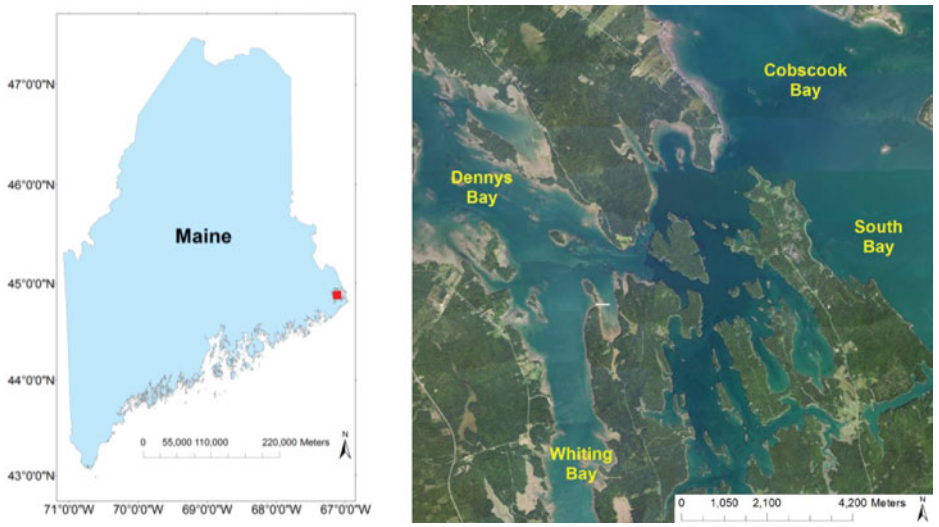

Figure 4. The survey area for ME1001.

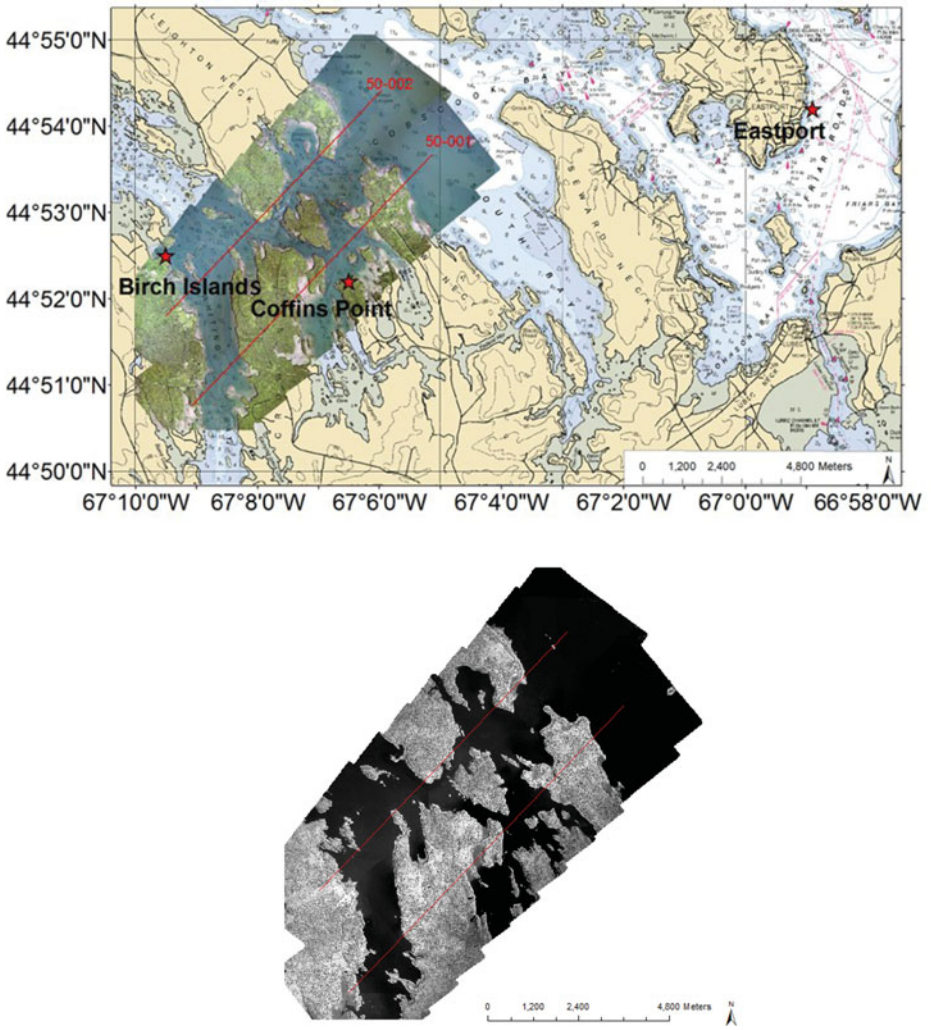

Figure 5. The mosaic imagery. (top) The natural color imagery overlaid on NOAA Chart (Office of Coast Survey 2014d); (bottom) the NIR imagery (The red lines are the two flight lines; stars denote the three tide gauge used in this survey).

methods of shoreline compilation (tide-coordinated and non-tide-coordinated) could be assessed.

Shoreline Uncertainty Based on Tide-Coordinated Imagery

The parameters for estimating the exterior orientation element uncertainty included the flying height over ground, 3048 m; camera focal length, 60.265 mm; pixel size on CCD chip, 6.8 μm; CCD length in the along-track direction, 5408 pixels; and CCD length in the across-track direction, 7212 pixels. In addition, a custom exterior orientation element report was output from POSPac, Applanix's software for direct georeferencing of airborne imaging sensors (Applanix 2014), containing not only the exterior orientation elements of

each image but also the standard uncertainties. A series of random numbers were generated from the probability distribution for each exterior orientation element as defined by the mean and the standard uncertainty. Then, the possible exterior orientation elements were applied to compute the ground coordinates of about 60 points in each image (100 points with equal distance interval were selected in each image. However, only about 60 points were brought into the computation due to 60% overlap.). The uncertainties of the ground coordinates were finally acquired by analyzing the spread in the position of all points. The X and Y uncertainties for the whole survey were found to be 0.61 m and 0.56 m, respectively, and thus the position uncertainty was 0.84 m according to DRMS formula.

The offset between the observed water level and the MLLW datum was acquired from the Tide Analysis Report (Table 1). The offsets relative to the MLLW datum were averaged for both subordinate stations at the GMT time of 14:06 and 14:18 as the offset based on tide-coordinate imagery (0.30 m).

With respect to the water level uncertainty, firstly, a typical value 0.022 m (personal communication, Lijuan Huang, NOAA/NOS/CO-OPS/Hydro Planning Team, 2013) was used for the measurement uncertainty of gauge/sensor and processing uncertainty to refer the measurements to station datum. Second, NGS used the water level data of the EastPort station to analyze water level data of the two subordinate stations (Coffins Point and Birch Islands). The EastPort station was established in 1929, and it is a 19-year control station. Therefore, the tidal datum uncertainty for Eastport was assumed to be zero (NOAA 2010). Third, the uncertainty in the application of tidal or water level zoning was analyzed by comparing the water level data from the Tidal Analysis Report and the prediction based on harmonic constituents because the harmonic constituents account for more than 99% of the total water level energy in this region and the predicted data based on harmonic constituents can be used as an alternative observed data to calculate the uncertainty (personal communication, Lijuan Huang, NOAA/NOS/CO-OPS/Hydro Planning Team, 2013). CO-OPS provided the predicted data based on harmonic constituents for Coffins Point and the predicted data based on four time and range correction parameters for Birch Islands. Therefore, the tidal data for Coffins Point was analyzed, and its uncertainty was treated as the tidal zoning uncertainty for the whole survey area. The tidal zoning uncertainty was 0.05 m. Because only the data at four different times were analyzed, the small sample size could make the sample estimate of standard deviation be skewed and smaller than the population standard deviation. According to the values of the Student's t for four and infinite sample sizes at 68% confidence level, it would be expected that the value of the actual tidal zoning uncertainty is $\sim$1.2 times that of the tidal zoning uncertainty estimated by the four samples.

Due to lack of the compilation results based on tide-coordinate imagery from different compilers in the study area, the compiled land/water interface vectors from four compilers in the Fort Desoto, Florida project in 2003 (Parrish et al. 2005) was applied to estimate the horizontal human compilation uncertainty. The horizontal human compilation uncertainty was found to be 1.06 m. Given that the coastal area in the Maine site is more complex than that in Fort Desoto, the human compilation uncertainty for the Maine site may be greater than that for Fort Desoto. In addition, the small sample size may have resulted in the sample human compilation uncertainty being less than the population human compilation uncertainty. Therefore, it would be expected that the value of the actual tide-coordinated human compilation uncertainty for the Maine site is greater than $\sim$1.2 times that of the tide-coordinated human compilation uncertainty estimated by the four Fort Desoto compilation samples. However, we believe the value obtained is a reasonable first-order approximation

Figure 6. Two selected areas for uncertainty analysis overlaid on the non-tide-coordinated imagery.

of the tide-coordinated human compilation uncertainty, given the difficulty in obtaining shoreline of the same site generated independently by multiple, trained compilers.

After obtaining all these uncertainty components, transects at the interval of 2 m along shorelines were generated using the Digital Shoreline Analysis System (DSAS) utility developed by United States Geological Survey (USGS) (Thieler et al. 2009). The total horizontal uncertainty for each transect was estimated by converting the vertical uncertainty components to the horizontal uncertainty components. According to the statistical analysis, the standard uncertainty and the uncertainty at the 95% confidence level for the whole study area were 3.28 m and 4.77 m, respectively.

Shoreline Uncertainty Based on Non-Tide-Coordinated Imagery

For the compilation based on non-tide-coordinated imagery, the exterior orientation element uncertainty and the water level uncertainty were the same with those based on tide-coordinated imagery. In addition, nine compilers with different experience levels compiled the MHW shoreline from non-tide-coordinated imagery in two selected areas (Figure 6), and the compilation results were applied to analyze the human compilation uncertainty.

Two reference shorelines were firstly created, and then shoreline transects were generated perpendicular to the reference shorelines at 10 m spacing (Figure 7). The average of the compiled shorelines was treated as the shoreline without human compilation uncertainty, and then the RMS of all the compilers' uncertainties was computed in each transect.

Combined with the slope information along the two shorelines, the planimetric human compilation uncertainty was converted to the uncertainty in elevation. Figure 8 illustrates the relationship between the slope and the planimetric human compilation uncertainty. From the distribution of the points, it can be seen that unlike the tide-coordinated compilation, the horizontal human compilation uncertainty from non-tide-coordinated imagery

Figure 7. The reference shorelines (red lines) and transects (blue lines). Different colors in transects represent the maximum differences of the compilation results from the compilers (meters).

depends on the beach slope, because compilers compile the shoreline based on the elevation information. When the vertical human compilation uncertainty is fixed, the horizontal human compilation uncertainty will change with the beach slope.

The black line was the least-square fitted straight line based on the data of planimetric human compilation uncertainty and the slope. The slope of this fitted straight line, 0.44 m, was used as the elevation uncertainty corresponding to this level of planimetric compilation uncertainty. It would be expected that the value of the actual non-tide-coordinated human compilation uncertainty is ~1.06 times that estimated by the 9 Maine compilation samples by Student's t compensating.

The boundaries for the standard uncertainty and the uncertainty at the 95% confidence level are shown on the imagery (Figure 9). The two uncertainties for the whole survey area were 3.15 m and 6.73 m, respectively.

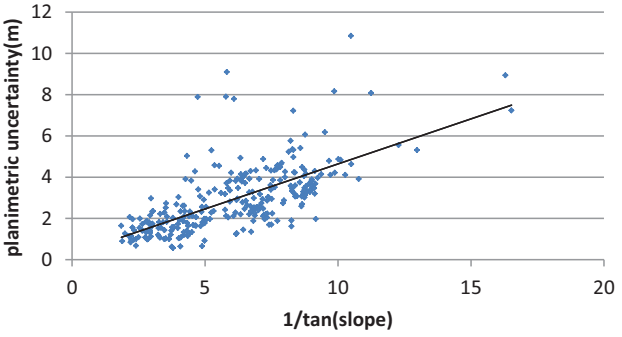

Figure 8. The relationship between the slope and the planimetric human compilation uncertainty.

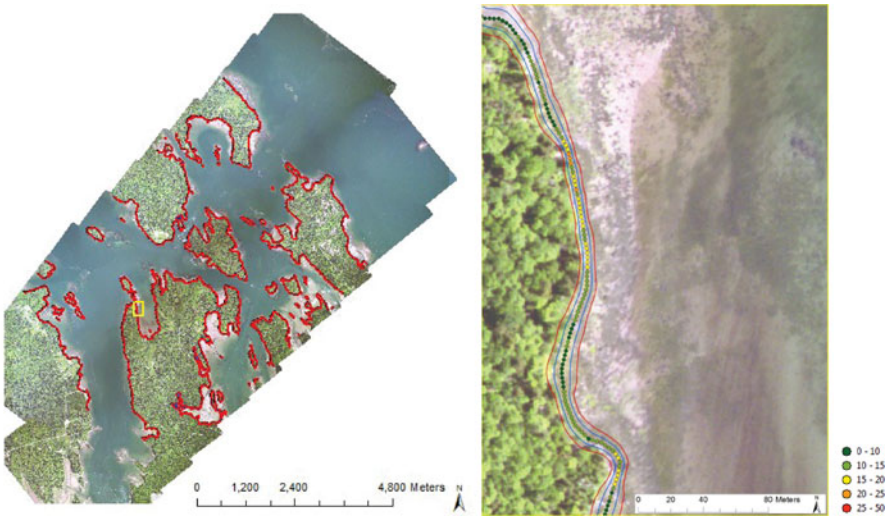

Figure 9. The uncertainty boundaries. The blue lines and the red lines represent the standard uncertainty and the uncertainty at the 95% confidence level, respectively. The black lines are the MHW shoreline. (Left) the imagery for the whole study area. (Right) the enlarged imagery for the yellow box in the left imagery. The points with different colors represent the slope in degree.

From Figure 9 (right), it can be seen that in a region with gentle slope the uncertainty is greater than that in a steep region. It can be concluded slope is an important factor which affects the shoreline uncertainty.

Discussion

Analysis of the results of this study led to the following observations:

- The positioning uncertainty caused by exterior orientation element uncertainty is affected by the photographic scale. The smaller the scale, the higher the point positioning uncertainty.
- The human compilation uncertainty was estimated by analyzing compilation results from different compilers. The estimated values for the two cases (tide-coordinated and non-tide-coordinated) in the experiment cannot be easily applied to any area or any set of compilers, and they should be adjusted based on different conditions, such as compiler's experience, image quality, and complexity of coastal region, for example, the human compilation uncertainty for rocky shorelines could be larger than that for tidal flats.
- For tide-coordinated compilation the offset between MHW/MLLW and observed water level has the main impact on the total uncertainty, followed by human compilation uncertainty, exterior orientation element uncertainty, and then water level uncertainty. For non-tide-coordinated compilation, the order is human compilation uncertainty, exterior orientation element uncertainty, and then water level uncertainty. In addition, human non-tide-coordinated compilation uncertainty is greater than the tide-coordinated one. Comparing the total standard uncertainties for the two cases, they are not very different from each other. This indicates that it may not be necessary to require a survey to be tide-coordinated. However, the

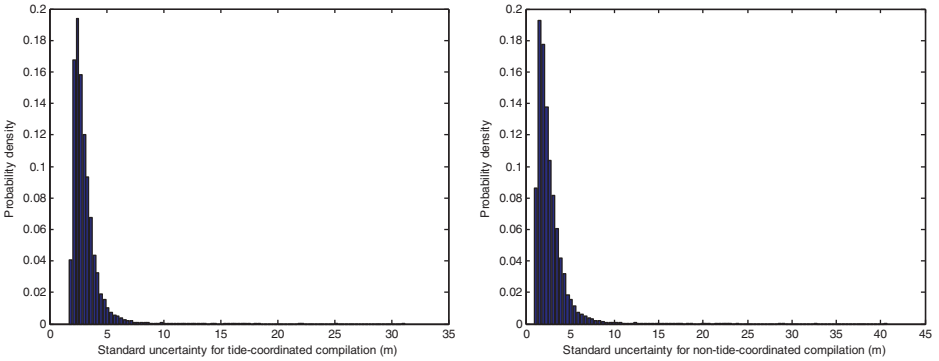

Figure 10. Distribution of standard uncertainties for tide-coordinated and non-tide-coordinated compilation.

shoreline TPU would need to be computed for many survey sites to determine if this is true in general, or only for this particular survey (Table 2).

- For the study area, the ranges of the standard uncertainties for tide-coordinated and non-tide-coordinated compilation are [1.72 m, 31.20 m] and [0.93 m, 40.78m] (Figure 10). The variability in the uncertainty is primarily attributable to slope variation (Figure 11). In areas with small slope, the uncertainty is higher. The upper limits of these TPU ranges are quite large. However, they are realistic, since in some sections of the study area the beach slope is extremely small, such as 0.66°. These upper limits of the uncertainty ranges should not be taken as a reflection of the standard uncertainty for the study area as a whole, but it is important to note that the uncertainty in a few localized areas can be significantly greater than the standard shoreline uncertainty for the survey.

Limitations of the methods included the small sample sizes for estimating the tide zoning uncertainty and human compilation uncertainty. This could have caused the estimated

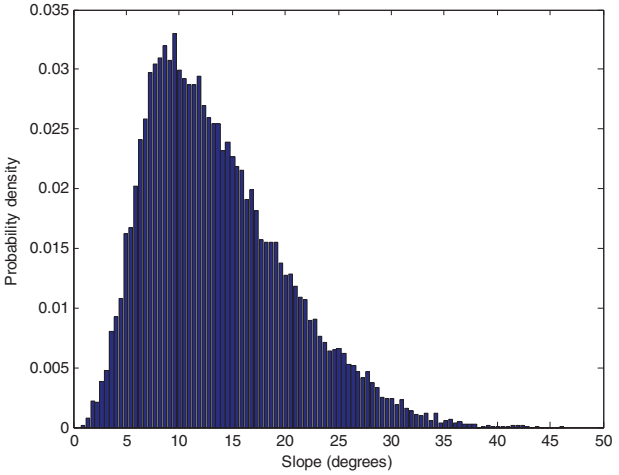

Figure 11. Distribution of slopes.

Table 2

The planimetric values (in meters) of each uncertainty component and the total uncertainties in the study area. (The tidal zoning uncertainty and the human compilation uncertainty were computed using their sample uncertainty values multiplied by their corresponding Student's t)

	Exterior orientation element uncertainty	The offset between MHW or MLLW datum and observed water level	Uncertainty in water level data			Human compilation uncertainty	Total uncertainty	
			Observation	Datum	Interpolation		Std	95%Cl
Tide-coordinated	0.84	1.96	0.15	0	0.39	1.26	3.28	4.77
Non-tide-coordinated	0.84	0	0.15	0	0.39	3.03	3.15	6.73

sample standard deviations to be skewed and to have slightly underestimated the population standard deviation. However, we believe the values obtained are plausible first-order approximations of the uncertainties, especially given the practical challenges in obtaining large samples for assessing these uncertainties.

Conclusion

This study has demonstrated a rigorous TPU model for a photogrammetrically derived shoreline based on the procedures used by NOAA NGS to map the national shoreline depicted on NOAA nautical charts. The model can be applied to populate the accuracy metadata required for digital geospatial data. This is especially beneficial in cases for which it is infeasible to acquire the reference data ("ground truth") necessary for empirical accuracy assessments. It also enables the spatial variation in shoreline uncertainty to be analyzed and displayed, which is beneficial in portraying the relationship between uncertainty and beach slope or other parameters.

The demand for both current and multitemporal shoreline data is likely to increase with heightened focus on climate change impacts, as well as the increasing population density in coastal areas. Providing reliable uncertainty estimates with the shoreline enables assessment of the uncertainty in models that use the shoreline data as an input. This includes, for example, models of coastal inundation due to sea level rise and marsh migration.

Another important aspect of the methods developed in this study is that they enable assessment of the relative contribution of each component uncertainty to the shoreline TPU. For the Maine site, using the tide-coordinated imagery methods the three most significant component uncertainties were 1) the offset between MHW/MLLW and the observed water level, 2) human compilation uncertainty, and 3) exterior orientation element uncertainty. In the non-tide-coordinated imagery case, the component uncertainties in order of significance were 1) human compilation uncertainty, 2) exterior orientation element uncertainty, and 3) uncertainty in water level data. This type of assessment is useful in improving the accuracy of shoreline data by focusing on reducing the component uncertainties that contribute most to the final shoreline positional uncertainty. Given plausible a priori estimates of beach slope and the component uncertainties, it is also possible to perform the TPU analysis before acquiring the aerial imagery for a project site. This can be useful in assessing whether project requirements are likely to be met with a specified set of mission parameters (e.g., flying height, tide tolerance threshold, DG system and camera specifications).

One area for possible future improvement in our methods is in modeling the human compilation uncertainty. Due to the difficulty in obtaining multiple shorelines compiled independently by different, experienced photogrammetrists, the sample size for estimating this component uncertainty was small. Also, in the tide-coordinated imagery case, the human compilation uncertainty was assessed using a different site than the Maine site used in this study. These factors could have led to a slight underestimate of the human compilation uncertainty in this study, although we believe the value obtained is a good first-order approximation. If future studies are able to include a larger number of compilers and wider range of source imagery, it may be possible to develop a more robust model of human compilation uncertainty, which includes additional variables, such as compiler experience level and image quality level.

Funding

This project was funded by the NOAA Joint Hydrographic Center grant NA05NOS4001153.

References

Alfugura, A., L. Billa, and B. Pradhan. 2011. Semi-automated procedures for shoreline extraction using single RADARSAT-1 SAR image. *Estuarine, Coastal and Shelf Science* 95(4): 395–400.

Applanix, 2014. POSPac MMS. Available at http://www.applanix.com/products/airborne/pospac-mms.html. Last accessed 8 May 2014.

Boak, E. H. and I. L. Turner. 2005. Shoreline definition and detection: A review. *Journal of Coastal Research* 21(4): 688–703.

Brennan, L. 2005. An uncertainty model for the tidal constituent and residual interpolation (TCARI) method of water level correction. MS Thesis. University of New Hampshire, Durham, NH.

Carter, C. H., D. J. Benson, and D. E. Guy, Jr. 1981. Shore protection structures: Effects on recession rates and beaches from the 1870s to the 1970s along the Ohio shore of Lake Erie. *Environmental Geology* 3: 353–362.

Cisternelli, M. and S. Gill. 2005. *Implementation of TCARI into NOS Hydrographic Survey Operations*. U.S. Hydro Conference, San Diego, CA March 2931.

Coastal Services Center. 2014. Digital Coast, Coastal Lidar. Available at https://csc.noaa.gov/digitalcoast/data/ coastallidar. Last accessed 8 May 2014.

CO-OPS. 2014. Hydrographic survey and shoreline mapping survey support. Available at http://tidesandcurrents.noaa. gov/hydro.html. Last accessed 8 May 2014.

Dieck, R. H. 2002. *Measurement Uncertainty: Methods and Applications.* 3rd ed. Research Triangle Park, NC: The Instrumentation, Systems and Automation Society.

Gibson, W. M. and S. K. Gill. 1999. Tides and water level requirements for NOS hydrographic surveys. *International Hydrographic Review* 76: 141–150.

Graham, D., M. Sault, and J. Bailey. 2003. National ocean service shoreline—past, present, and future. *Journal of Coastal Research* SI(38): 14–32.

Hess, K., R. Schmalz, C. Zervas, and W. Collier. 1999. Tidal constituent and residual interpolation (TCARI): A new method for the tidal correction of bathymetric data. Technical report, National Oceanic and Atmospheric Administration.

International Hydrographic Organization. 2008. *IHO Standards for Hydrographic Surveys.* 5th ed. Monaco: International Hydrographic Bureau.

Leatherman, S. P. and F. J. Anders. 1999. Mapping and managing coastal erosion hazards in New York. *Journal of Coastal Research* Special Issue No. 28: 34–42.

Li, R., R. Ma, and K. Di. 2002. Digital tide-coordinated shoreline. *Marine Geodesy* 25(1/2): 27–36.

Morton, R. A. and F. M. Speed. 1998. Evaluation of shorelines and legal boundaries controlled by water levels on sandy beaches. *Journal of Coastal Research* 14(4): 1373–1384.

National Geodetic Survey. 2014a. Remote sensing division coastal mapping program. Available at http://www.ngs.noaa. gov/RSD/cmp.shtml. Last accessed 8 May 2014.

National Geodetic Survey. 2014b. Coastal and shoreline change analysis program. Available at http://www.ngs.noaa.gov/ RSD/cscap.shtml. Last accessed 8 May 2014.

NOAA. 2010. *Technical considerations for use of geospatial data in sea level change mapping and assessment.* Silver Spring, MD: National Oceanic and Atmospheric Administration, National Ocean Service, NOAA Technical Report NOS 2010-01.

Office of Coast Survey. 2014a. Datums and transformations. Available at http://www.nauticalcharts.noaa.gov/csdl/ learn_datum.html. Last accessed 8 May 2014.

Office of Coast Survey. 2014b. Tidal corrector application (TCARI). Available at http://www.nauticalcharts.noaa.gov/csdl/tcari.html. Last accessed 8 May 2014.

Office of Coast Survey. 2014c. Field procedures manual. Available at http://www.nauticalcharts.noaa.gov/hsd/fpm/ FPM_2013_Final_5_3_13.pdf. Last accessed 8 May 2014.

Office of Coast Survey. 2014d. Chart 13394. Available at http://www.charts.noaa.gov/OnLineViewer/13394.shtml. Last accessed 8 May 2014.

Pajak, M. J. and S. P. Leatherman. 2002. The high water line as shoreline indicator. *Journal of Coastal Research* 18(2): 329–337.

Papadopoulos, C. and H. Yeung. 2001. Uncertainty estimation and Monte Carlo simulation method. *Flow Measurement and Instrumentation* 12: 291–298.

Parrish, C. E., M. Sault, S. A. White, and J. Sellars. 2005. Empirical analysis of aerial camera filters for shoreline mapping. *Proceedings of the ASPRS 2005 Annual Conference*, 7–11 March, Baltimore, MD.

Sabins, F. F. 1986. *Remote Sensing: Principles and Interpretation.* 2nd ed. New York: W.H. Freeman and Company.

Shalowitz, A. L. 1964. Shore and sea boundaries. U.S. Department of Commerce, U.S. Coast and Geodetic Survey.

Smith, J. T. Jr. 1978. NOS photographic operations for photobathymetry. *Proceedings Coastal Mapping Symposium, American Society of Photogrammetry*, 14–16 August, Rockville, MD.

Smith, G. L. and G. A. Zarillo. 1990. Calculating long-term shoreline recession rates using aerial photographic and beach profiling techniques. *Journal of Coastal Research* 6(1): 111–120.

Stafford, D. B. and J. Langfelder. 1971. Air photo survey of coastal erosion. *Photogrammetric Engineering* 37(6): 565–575.

Stockdon, H. F., A. H. Sallenger, J. H. List, and R. A. Holman. 2002. Estimation of shoreline position and change using airborne topographic Lidar data. *Journal of Coastal Research* 18: 502–513.

Thieler, E. R., E. A. Himmelstoss, J. L. Zichichi, and A. Ergul. 2009. Digital shoreline analysis system (DSAS) version 4.0—an ArcGIS extension for calculating shoreline change. U.S. Geological Survey Open-File Report 2008-1278.

White, S. A., C. E. Parrish, B. R. Calder, S. Pe'eri, and Y. Rzhanov. 2011. Lidar-derived national shoreline: Empirical and stochastic uncertainty analyses. *Journal of Coastal Research* SI(62): 62–74.

Woolard, J. W., M. Aslaksen, J. L.T. Longenecker, and A. Ryerson. 2003. Shoreline mapping from airborne LiDAR in Shilshole Bay, Washington. *Proceedings of National Oceanic and Atmospheric Administration (NOAA) National Ocean Service (NOS), U.S. Hydrographic Conference.*

Yuan, X. X. and X. P. Zhang. 2008. Theoretical accuracy of direct georeferencing with position and orientation system in aerial photogrammetry. *Proceedings of the International Archives of the Photogrammetry, Remote Sensing and Spatial Information Sciences*, 3–11 July, Beijing.

Zhang, X. P. and X. X. Yuan. 2008. Effects of exterior orientation elements on direct georeferencing in POS-supported aerial photogrammetry. *Proceedings of the 8th International Symposium on Spatial Accuracy Assessment in Natural Resources and Environmental Sciences*, 25–27 June, Shanghai.